THE UNIVERSITY OF RHODE ISLAND

Graduate School of Oceanography Faculty Publications

Graduate School of Oceanography

2001

A Characterization of the North Atlantic STMW Layer Climatology Using *World Ocean Atlas 1994* Data

Michael A. Alfultis
University of Rhode Island

Peter C. Cornillon
University of Rhode Island, pcornillon@uri.edu

A Characterization of the North Atlantic STMW Layer Climatology Using *World Ocean Atlas 1994* Data

A Characterization of the North Atlantic STMW Layer Climatology Using *World Ocean Atlas 1994* Data

MICHAEL A. ALFULTIS* AND PETER CORNILLON

Graduate School of Oceanography, University of Rhode Island, Narragansett, Rhode Island

ABSTRACT

The North Atlantic Subtropical Mode Water (STMW) layer was identified based on its temperature, large thickness, and small temperature gradient. Comparisons between this method and identifying the STMW layer using a density-based (i.e., potential vorticity) criteria indicate that this method successfully identifies the STMW layer as the remnant of the previous winter's convective mixing. By using this temperature-based characterization of the STMW layer, this method was able to develop a climatology using the large number of expendable bathythermographs (XBTs) deployed between 1968 and 1988, and contained in the *World Ocean Atlas 1994* historical hydrographic database. From this climatology, the STMW layer that is the remnant of the previous winter's convective activity is typically found between 175 and 450 m, has an average temperature near 18°C, and has a mean temperature gradient of 0.5°C $(100 \text{ m})^{-1}$. Comparisons of the STMW temperature, thickness, and temperature gradient characteristics in this climatology agree with other observations of the North Atlantic STMW layer.

1. Introduction

Subtropical Mode Waters (STMW) are water masses located between the seasonal and main thermoclines in the northwestern and central portions of subtropical gyres (Schroeder et al. 1959; Suga and Hanawa 1990; Qiu and Joyce 1992). STMWs have been identified in the North Pacific (Masuzawa 1969), North Atlantic (Worthington 1959), South Pacific (Roemmich and Cornuelle 1992), South Atlantic (Provost et al. 1999), and Indian Ocean (Belkin and Gordon 1996) subtropical gyres. These water masses are generally understood to form in late winter when atmospheric cooling removes the seasonal stratification, exposing thick well-mixed layers on the equatorward side of separated western boundary currents to further cooling and convective mixing (McCartney 1982; Talley and Raymer 1982; Ebbesmeyer and Lindstrom 1986; Suga and Hanawa 1990; Qiu and Joyce 1992; Roemmich and Cornuelle 1992). Although the regions of strongest wintertime atmospheric cooling and convective mixing are limited to the northwestern portions of the subtropical gyre, STMW can be found throughout much of the subtropical

gyre due to advection (Worthington 1959; McCartney et al. 1980; McCartney 1982; Talley and Raymer 1982; Ebbesmeyer and Lindstrom 1986; Bingham 1992; Hall and Fofonoff 1993; Klein and Hogg 1996).

North Atlantic STMW (NASTMW) is classically defined by temperatures ranging from 17.6° to 18.2°C (Worthington 1959), salinities 36.4 to 36.6 practical salinity units (psu; Schroeder et al. 1959; Worthington 1959), and potential densities at its core ~26.4 kg m^{-3} (Worthington 1959; Talley and Raymer 1982). Since the NASTMW core temperature is approximately 18°C, it is often referred to as "Eighteen Degree Water" (Schroeder et al. 1959; Worthington 1959; Ebbesmeyer and Lindstrom 1986). NASTMW seems most prevalent in a region extending from the Gulf Stream south to 30°N and east to 45°W (Worthington 1959; Istoshin 1961; McCartney 1982; Ebbesmeyer and Lindstrom 1986), but its characteristics can be observed as far south as 20°N and east of 45°W (Istoshin 1961).

The vertical homogeneity of the STMW layer is its most widely discussed characteristic. However, when discussing the degree of stratification of the STMW layer, it is important to distinguish the STMW layer in winter when it is exposed to atmospheric cooling and convective mixing from the STMW layer when it is isolated from atmospheric forcing. While it is experiencing convective mixing in winter, the STMW layer's temperature and salinity are vertically homogeneous (Worthington 1959; Istoshin 1961; Worthington 1972; Leetmaa 1977; Worthington 1977; Hall and Fofonoff

---

* Current affiliation: Department of Science, U.S. Coast Guard Academy, New London, Connecticut.

Corresponding author address: CDR Michael Alfultis, Department of Science, US Coast Guard Academy, 27 Mohegan Avenue, New London, CT 06320-8101.
E-mail: MAlfultis@cga.uscg.mil

1993). However, once the STMW layer is isolated from atmospheric forcing with the return of the seasonal stratification, it is no longer strictly vertically homogeneous (Schroeder et al. 1959; Worthington 1972; Leetmaa 1977; Worthington 1977; McCartney et al. 1980). Rather, it has a small temperature gradient ranging from 0.03° to 0.08°C $(100 \text{ m})^{-1}$ in NASTMW recently exposed to atmospheric cooling (Worthington 1977; McCartney et al. 1980), and 0.7° to 0.8°C $(100 \text{ m})^{-1}$ in NASTMW that has had no recent exposure to atmospheric cooling (Leetmaa 1977; Worthington 1977; Taft et al. 1986; Klein and Hogg 1996). (A positive temperature gradient represents temperatures decreasing as depth increases.) However, the variation in time and space of this vertical temperature gradient is not well known.

Since, these small vertical temperature gradients represent the stratification minimum between the seasonal and main pycnoclines, the STMW layer can also be identified by its small vertical density gradient (McCartney 1982; Talley and Raymer 1982; Suga and Hanawa 1995). However, when a water parcel circulates through the subtropical gyre, its vertical density gradient changes to conserve its potential vorticity (McCartney 1982; Talley and Raymer 1982). If relative vorticity is neglected, the potential vorticity simplifies to a conservation of thickness (or vortex stretching) between isopycnals:

$$\frac{f}{\rho_\theta}\frac{\partial \sigma_\theta}{\partial z}. \qquad (1)$$

Therefore, the potential vorticity, like the vertical density gradient, has a minimum in the STMW layer, and, assuming mixing and relative vorticity can be neglected, has the added advantage of being a conservative tracer. Because of this, the potential vorticity has been frequently used to identify the STMW layer (McCartney 1982; Talley and Raymer 1982; Ebbesmeyer and Lindstrom 1986; Klein and Hogg 1996). The potential vorticity values for the NASTMW layer range from less than 2.5×10^{-11} m^{-1} s^{-1} in recently formed STMW up to 9×10^{-11} m^{-1} s^{-1} in STMW with no recent exposure to the atmosphere (McCartney 1982; Talley and Raymer 1982; Ebbesmeyer and Lindstrom 1986; Hall and Fofonoff 1993). For comparison, Ebbesmeyer and Lindstrom (1986) found the potential vorticity values of the seasonal and main pycnoclines to be greater than 50×10^{-11} and 15×10^{-11} m^{-1} s^{-1}, respectively. Again, these values indicate that although the STMW layer coincides with the stratification minimum between the seasonal and main pycnoclines, it is not truly vertically homogeneous, but has a density gradient associated with it.

The hydrographic studies discussed here have increased our understanding of the three-dimensional structure of the STMW layer, but there has been no previous examination of the long-term mean distribution of NASTMW layer properties based on in situ hydrographic data. In addition, there has been very little previous work using hydrographic data to examine how the NASTMW properties vary annually and interannually. Previous studies of NASTMW layer properties and their interannual variability were based on the long-term hydrographic dataset collected in the vicinity of Bermuda (32°10′N, 64°30′W) by the Bermuda Biological Station's vessel *Panulirus,* a single point in space (Talley and Raymer 1982; Joyce and Robbins 1996; Klein and Hogg 1996), and numerical model results (Marsh and New 1996; Hazeleger and Drijfhout 1998). The goal here is to develop methodologies for identifying NASTMW based on its temperature, thickness, and temperature gradient; and constructing a climatology of NASTMW properties from hydrographic station, conductivity–temperature–depth (CTD), and expendable bathythermograph (XBT) data, similar to the climatology for the North Pacific STMW layer constructed by Yasuda and Hanawa (1997). This climatology will then be applied here to examine more closely the vertical and horizontal variations in the NASTMW thickness, temperature, and temperature gradient. Following a description of the data types used to form the climatology, the methods used to identify the NASTMW layer, determine the NASTMW layer characteristics, and assemble the climatology will be discussed. After the data and methods are described, the vertical and horizontal variations of the STMW properties highlighted by the climatology will be discussed. The companion to this paper (Alfultis and Cornillon 2001) will then use the same hydrographic dataset to examine the annual and interannual variability in the STMW layer depth, temperature, and temperature gradient.

2. Data sources

The major source of hydrographic data for this study was the *World Ocean Atlas 1994* (Levitus and Boyer 1994, hereafter *WOA94*), produced by the National Oceanographic Data Center's (NODC) Ocean Climate Laboratory (OCL). Each Station, CTD, and bathythermograph profile in the *WOA94* dataset was recorded in two formats: the observed data at the actual observation depths (''observed level'' data) and data interpolated to standard depth levels (''standard level'' data). Quality control procedures were performed on each profile before and after interpolation to standard levels. The observed level data were chosen for determining the STMW properties in this study in order to maximize the vertical sampling in the STMW layer, which extends from ~200 to ~400 m. The standard level data is only provided at every 50 or 100 m at these depth levels, while the vertical sampling in the observed level data was either based on the inflection points in the temperature profile or every ~25 m (on average).

The second source of hydrographic data for this study was a set of hydrographic profiles collected along 15 repeated sections as part of the Russian Long-term Re-

search on Hydrometeorological Anomalies and Sections research programs (Lappo et al. 1995). The data made available for this study were temperature and salinity interpolated to standard levels. Five of these sections transitted the subtropical gyre and, therefore, were likely to sample the STMW layer. There was a total number of 2452 profiles collected along these sections in the subtropical gyre region (20°N to 45°N, 80°W to 40°W), far less than the number of *WOA94* profiles in the same region. However, since these sections have been repeated several times over periods ranging from seven to fourteen years, they have an added importance when looking at interannual variability of the STMW characteristics.

3. Data processing

The first step in processing the data entailed selecting those station, CTD, and XBT profiles in the region from 20°N to 45°N and 80°W to 40°W with maximum depths greater than 300 m. The selected *WOA94* profiles were then screened using preliminary quality control criteria. Duplicate profiles and profiles flagged by the NODC OCL as coming from cruises with consistently poor quality control were removed. Any observation in a profile flagged by the OCL as an outlier, a large temperature inversion, or large temperature gradient was removed from the profile. Next, only *WOA94* and Russian profiles in the subtropical gyre, seaward of the Gulf Stream, north of 25°N and west of 40°W, hence likely to have sampled the STMW layer, were selected. The depth of the 17°C isotherm was used as an indicator of the offshore side of the Gulf Stream (Alfultis 1997).

The OCL's drop-rate correction was then applied to all *WOA94* XBTs shallower than 800 m to correct for the fact that, in general, they fall faster than the published drop rates (Hanawa and Yoritaka 1987; Singer 1990; Hanawa and Yoshikawa 1991; Hallock and Teague 1992; Hanawa et al. 1995). Spikes thought to result from instrument noise were then removed from the XBT profiles, and "large" density inversions were removed from all station and CTD profiles. Finally, profiles with inadequate vertical sampling at typical STMW depths were eliminated from the dataset (Alfultis 1997).

The results of this screening and processing are summarized in the first ten rows of Table 1.

4. Identifying STMW layer

The STMW layer can exist in one of four different configurations (Fig. 1):

1) An STMW layer with all of the seasonal stratification removed and a thickening mixed layer above. Here, the top of the STMW layer is beginning to be renewed by the convective mixing that is deepening the winter mixed layer. Therefore, in this case, there are in fact two STMW layers—a new STMW layer

TABLE 1. Summary of data processing.

	CTD	Station	XBT	Russian
No. profiles in region 20°– 45°N, 80°–40°W	21 328	77 928	213 837	2452
w/depth <300 m	12 861	50 699	68 809	32
Duplicates	319	2184	1513	4
Missing temp/salinity data	112	770	0	0
Failed QC	34	706	7	0
Inadequate data 100–500 m	80	1351		0
Max temp <17°C	2029	7081	15 127	227
Depth 17°C isotherm <350 m	2124	6678	42 267	767
>1 Density inversion	8	13	—	0
No. profiles tested for STMW layer	3761	8446	86 114	1422
No. STMW layer	518	1915	22 586	164
STMW layer rms >0.19	1	10	421	1
No. profiles w/STMW layer	3242	6521	63 107	1257

beginning to form as the mixed layer continues to deepen, and the older STMW layer below. The temperature gradients in the older STMW layer will be slightly larger than in the mixed layer, but they will still be much smaller than the temperature gradients found in the permanent thermocline below.

2) Convective mixing has completely renewed/ventilated the STMW layer. In this case, the top of the STMW layer is the sea surface and the bottom of the STMW layer equals the depth of the winter mixed layer.

3) A single STMW layer with an overlying seasonal thermocline and mixed layer. In this case, the STMW layer will be the layer of minimum temperature gradients between the more stratified seasonal and permanent thermoclines.

4) A multiple-layer STMW layer between the seasonal and permanent thermoclines. This type of STMW layer would form when convective mixing the previous winter did not completely renew/ventilate the preexisting STMW layer (i.e., the first configuration), and the seasonal thermocline returns with the warming of the surface waters in spring.

The STMW layer is commonly identified as the potential vorticity (i.e., the stratification) minimum between the seasonal and permanent pycnoclines (McCartney 1982; Talley and Raymer 1982; Ebbesmeyer and Lindstrom 1986; Klein and Hogg 1996). Unfortunately, however, the spatial and temporal distributions of station and CTD profiles are insufficient to accurately determine the evolution of STMW properties annually and/or interannually in the region of interest (Alfultis 1997). In comparing XBT's with station profiles in the vicinity of Bermuda, Klein and Hogg (1996) found that temperature gradients less than $0.8°\text{C} \ (100 \ \text{m})^{-1}$ corresponded with the stratification minimum from potential vorticity. Since there is an order of magnitude greater number of XBT profiles than station and CTD profiles in the *WOA94* dataset, we developed a technique to
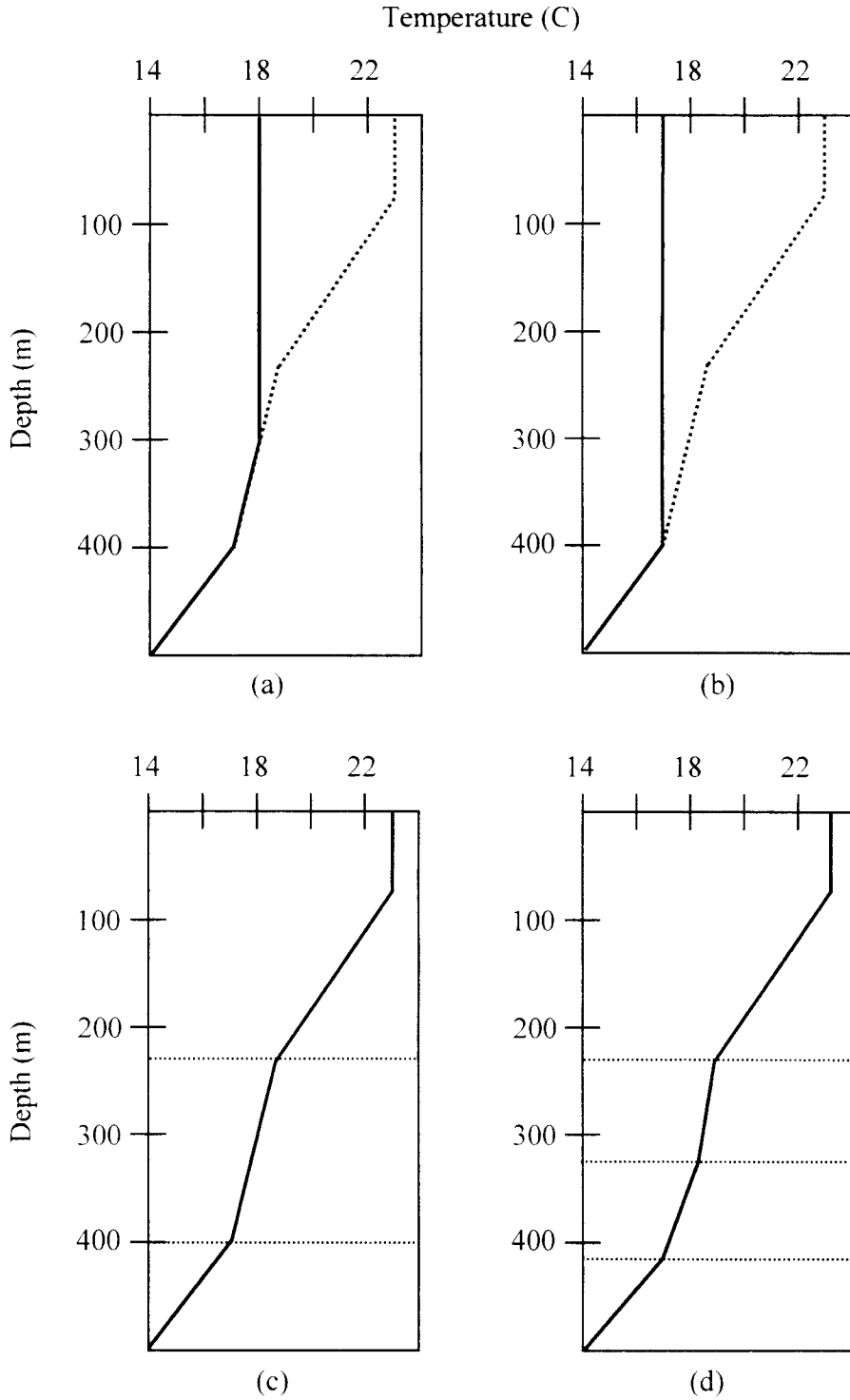
FIG. 1. Four possible STMW configurations: (a) wintertime convective mixing partially penetrates and renews the layer, (b) wintertime convective mixing renews entire layer, (c) single STMW layer between seasonal and permanent thermoclines, and (d) multiple-layer STMW layer between seasonal and permanent thermoclines.

identify and characterize the STMW layer which relied solely on temperature profiles. As we will discuss later, the method used here could identify the STMW layer in the first three cases. This method would identify the two STMW layers in the last case as a single, thick STMW layer because it could not distinguish the newly formed STMW layer from the preexisting SMTW layer due the small differences in the temperature and temperature gradient of each layer.

Once the appropriate profiles were selected and initially processed (section 3), the mixed layer temperature and depth were determined. Following Hanawa and Hoshino (1988) and Suga and Hanawa (1990), the temperature recorded at the depth closest to 10 m was chosen as the mixed layer temperature. No mixed layer was found for profiles with no observation shallower than 20 m.

The mixed layer base is commonly identified as the depth where the temperature is 1.0°C less than the surface temperature (Lamb 1984; Hanawa and Hoshino 1988; Suga et al. 1989; Suga and Hanawa 1990). However, in the first STMW configuration where the seasonal thermocline is absent, this criterion tends to identify the bottom of the older STMW layer as the bottom of the mixed layer due to the small temperature differences between the old STMW layer top (the actual mixed layer base) and the old STMW layer bottom. In this study, the mixed layer was distinguished from the STMW layer underneath by the difference in the temperature gradients in each layer (Alfultis 1997).

Once the mixed layer was determined, the STMW layer was identified based on its temperature, temperature gradient, and thickness. A profile was said to have a STMW layer if it met one or both of two sets of criteria. First, the deepest layer, at least 95 m thick, with temperatures between 16.5° and 19.5°C, and temperature gradients between adjacent pairs of points less than or equal to 0.95°C (100 m)$^{-1}$ was identified as a candidate STMW layer. The second method identified as a possible STMW layer the thickest layer exceeding 95 m with temperatures between 16.5° and 19.5°C and a temperature difference through the layer less than or equal to 0.95°C. These values were chosen based on Talley and Raymer (1982), Hall and Fofonoff (1993), and Klein and Hogg (1996) to identify the general part of the water column containing STMW without biasing any subsequent results. The second method had the advantage of being less sensitive to noise in the profile than the first method. When the layers identified by the two methods differed, the thickest layer encompassing both layers was chosen. Two tests were then performed on points in the vicinity of the top and bottom of the candidate STMW layer to determine if adding or removing these points would make a more uniform STMW layer (Alfultis 1997). If neither method could identify a layer with these characteristics, the profile was rejected.

Figure 2 illustrates the performance of the entire STMW layer selection process outlined above as applied to four XBT profiles in three of the four STMW configurations defined at the beginning of this section. The XBT profile in the upper left panel has a deepening mixed layer on top of a STMW layer (case 1). The mean temperature gradient through the STMW layer is 0.53°C (100 m)$^{-1}$, while the temperature gradient between the bottom of the mixed layer and the STMW layer top is 0.96°C (100 m)$^{-1}$. The XBT profile in the upper right panel is that of a newly formed STMW layer with a temperature very near 18°C and a depth of 450 m (case 2). The temperature gradients under this layer are all greater than 1.0°C (100 m)$^{-1}$. Given the small temperature gradients in the STMW layer in the lower left panel [0.15°C (100 m)$^{-1}$] and the time of year (early spring), this is most likely a STMW layer that was just formed, and the surface layers are beginning to become warmed and restratified (case 3). The temperature gradients between the shallow mixed layer and the STMW layer, as well as below the STMW layer, are greater than 1.0°C (100 m)$^{-1}$. Based on the date and small temperature gradients through the STMW layer [average temperature gradient is 0.19°C (100 m)$^{-1}$, the XBT profile in the lower right panel is another example of a recently formed STMW layer between a developing seasonal thermocline and the top of the main thermocline (case 3).

The method developed here worked reasonably well when the seasonal thermocline was present (June–January), and the STMW layer was in the third configuration, as in the lower two panels of Fig. 2. The three primary reasons for an incorrect determination of the STMW layer were noise in the observed temperatures, the presence of multiple STMW layers (such as a newly formed STMW layer sitting on top of an older layer with a slightly higher gradient), or a temperature inversion in the STMW layer. The left panel of Fig. 3 is an example of the second case. The method used here identified a single STMW layer extending from ~200 m to ~575 m. Visual inspection suggests there were two STMW layers in this profile, a newly formed STMW layer sitting on top of a remnant of a previously formed STMW layer. The upper, more recently formed, portion of the STMW layer with a temperature gradient of ~0.5°C (100 m)$^{-1}$ extends from approximately 200 to 400 m. The lower, older layer, with a temperature gradient of ~0.9°C (100 m)$^{-1}$ extends from 400 to 575 m. The temperature gradients of both layers were within the standard error of each other and were included in one layer. An example of the third case, is shown in the right panel of Fig. 3 where a temperature inversion occurs at 250 m, in the middle of a STMW layer identified using this method as extending from ~130 to ~375 m (~245 m thick). Visual inspection indicates the STMW layer is actually deeper (top ~180 m) and thinner (~145 m).

In cases of incorrect STMW layer determination, the rms error between the best-fit line and the actual data
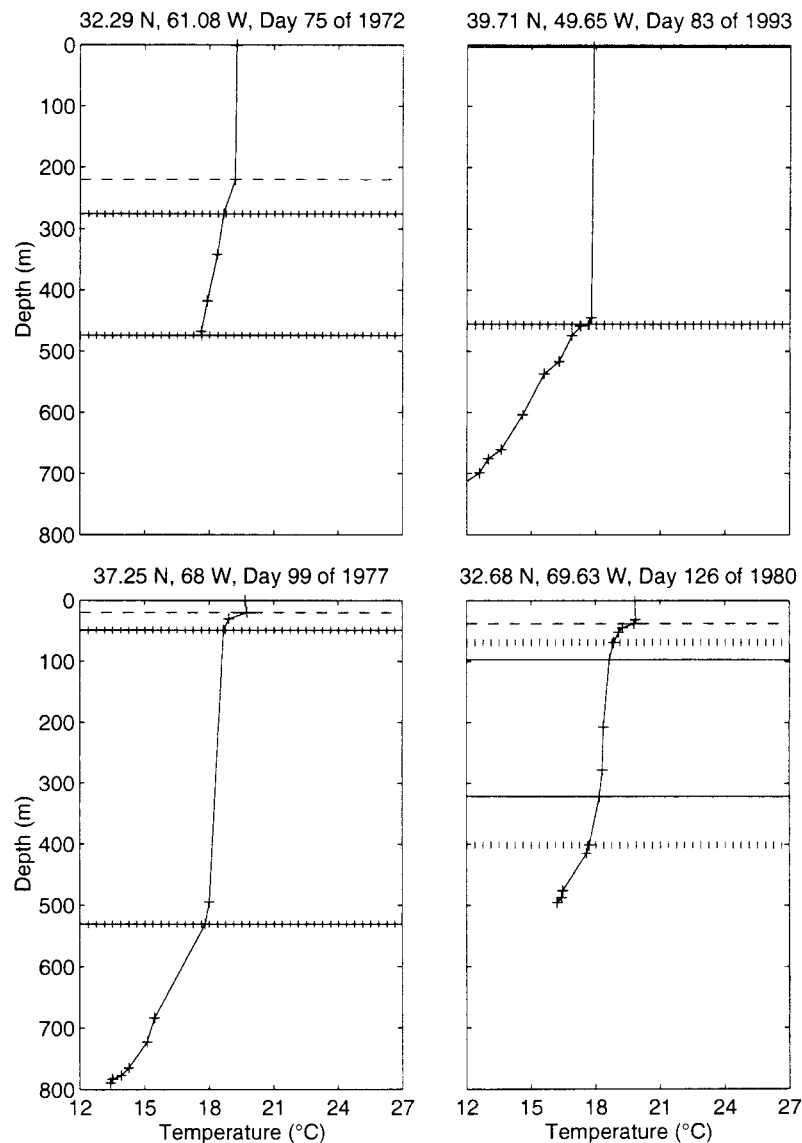
FIG. 2. Four examples of identifying the STMW layer. The dashed line represents the mixed layer base. The short vertical lines represent the initially identified STMW layer. The solid line represents the STMW layer after the two uniformity tests.

points in the STMW layer would be large. In the first example, the rms error was 0.12°C, and in the second example it was 0.16°C. Ninety-four percent of the profiles had an rms error in the STMW layer less than 0.1°C. These profiles were able to reliably find the STMW layer top and bottom. One percent of the profiles had an rms error in the STMW layer greater than 0.2°C. These profiles were manually examined. If an STMW layer thicker than 100 m could be correctly identified, the STMW layer top and bottom were corrected. If no such layer could be found, the profile was rejected. Of the 549 profiles inspected, 217 were corrected and retained.

Five percent of the profiles had an rms error between 0.1° and 0.2°C. Most of these profiles were collected in

February through June. As illustrated with the two examples in Fig. 3, these profiles were able to find the STMW layer top and bottom, but there is some anomaly within the STMW layer, such as noise, a second STMW layer, or a temperature inversion, which made the standard error from the mean of the temperature gradients within the layer relatively large. This prevented the end points from being correctly tested and eliminated. In both of the cases shown in Fig. 3; temperature gradients between the end points were within the large standard error of the selected layer and were therefore retained. However, in these cases (where the rms error is between 0.1° and 0.2°C), this method found reasonably close limits for the top and bottom of the layer of minimum
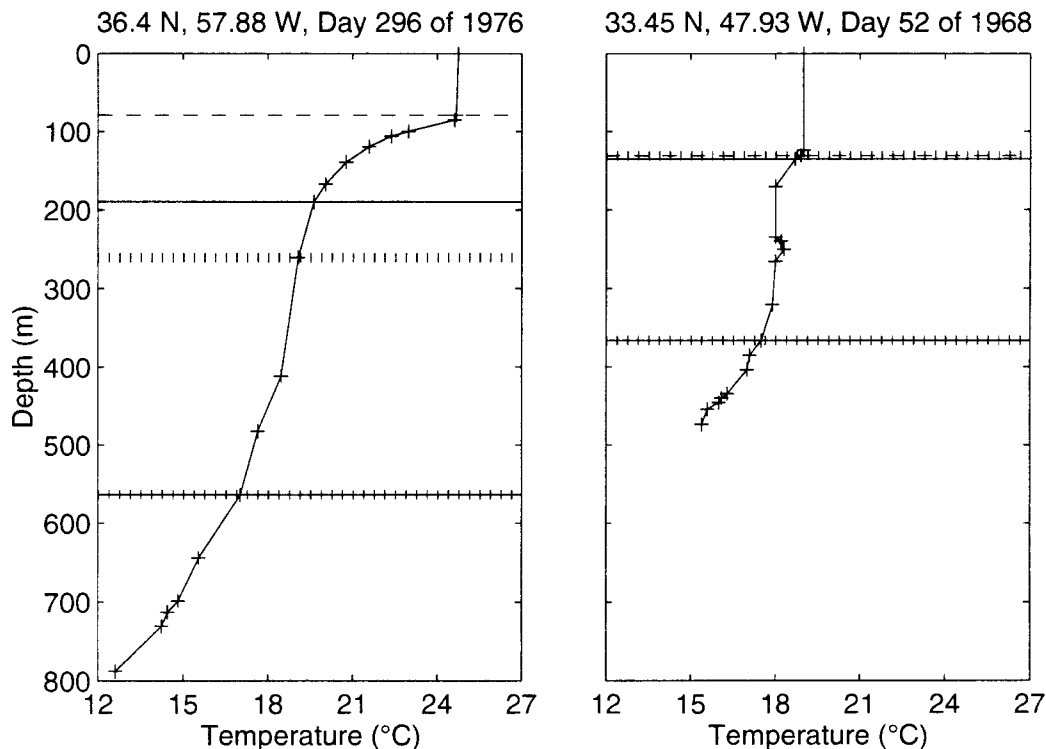
FIG. 3. Two examples of errors in identifying the STMW layer. The dashed line represents the mixed layer base. The short vertical lines represent the initially identified STMW layer. The solid line represents the STMW layer after the two uniformity tests.

stratification between the mixed layer and permanent thermocline.

Table 1 shows the flow of data through these data processing steps. Most of the profiles rejected were either too shallow, outside of the subtropical gyre, or contained no STMW layer. Approximately 30% of the XBT profiles, 10% of the station data, and 15% of the CTDs in the region were used to construct the STMW climatology. Figure 4 shows the spatial distribution of the three different data types used to construct the STMW climatology.

a. Determining STMW layer characteristics

The STMW layer properties determined here are the depth of the top and bottom of the STMW layer, the temperature at the top and bottom of the layer, and the temperature gradient through the layer. The top of the STMW layer was identified as the shallowest of the points in the most uniform layer. Next, a least squares line was fit to the data points in the most uniform layer. The mean temperature gradient through the STMW layer was determined from the slope of this best-fit line.

The depth and temperature at the bottom of the STMW layer were determined when the maximum depth of the profile was greater than 600 m, provided the bottom of the STMW layer was found before the end of the profile. The potential vorticity of the STMW

layer was also determined from station and CTD profiles meeting these two criteria. The potential vorticity of the STMW layer was calculated neglecting relative vorticity and using

$$\frac{f}{\rho_\theta} \frac{\Delta \sigma_\theta}{\Delta z}, \qquad (2)$$

where ρ_θ = the middensity of the layer, and $\Delta \sigma_\theta / \Delta z$ was estimated from the slope of the best-fit line to the potential density, values in the STMW layer ρ_θ and σ_θ are both determined from temperature and salinity, hence the requirement for Station and CTD profiles. Since XBT profiles constitute the bulk of the data in the *WOA94* and most of these ($\sim$⅔) are shallower than 600 m, the uncertainties in the properties at the bottom of the STMW layer will be larger than the properties at the top of the layer. In addition, there is not enough station and CTD data to construct a climatology of the STMW layer's potential vorticity. The STMW layer potential vorticity was determined to compare the method used here to identify the STMW layer with the STMW layer determined from the stratification–potential vorticity minimum.

b. Temperature gradient minimum–potential vorticity minimum comparisons

The STMW layer is commonly identified based on its stratification minimum using the vortex stretching

WOA XBT Data

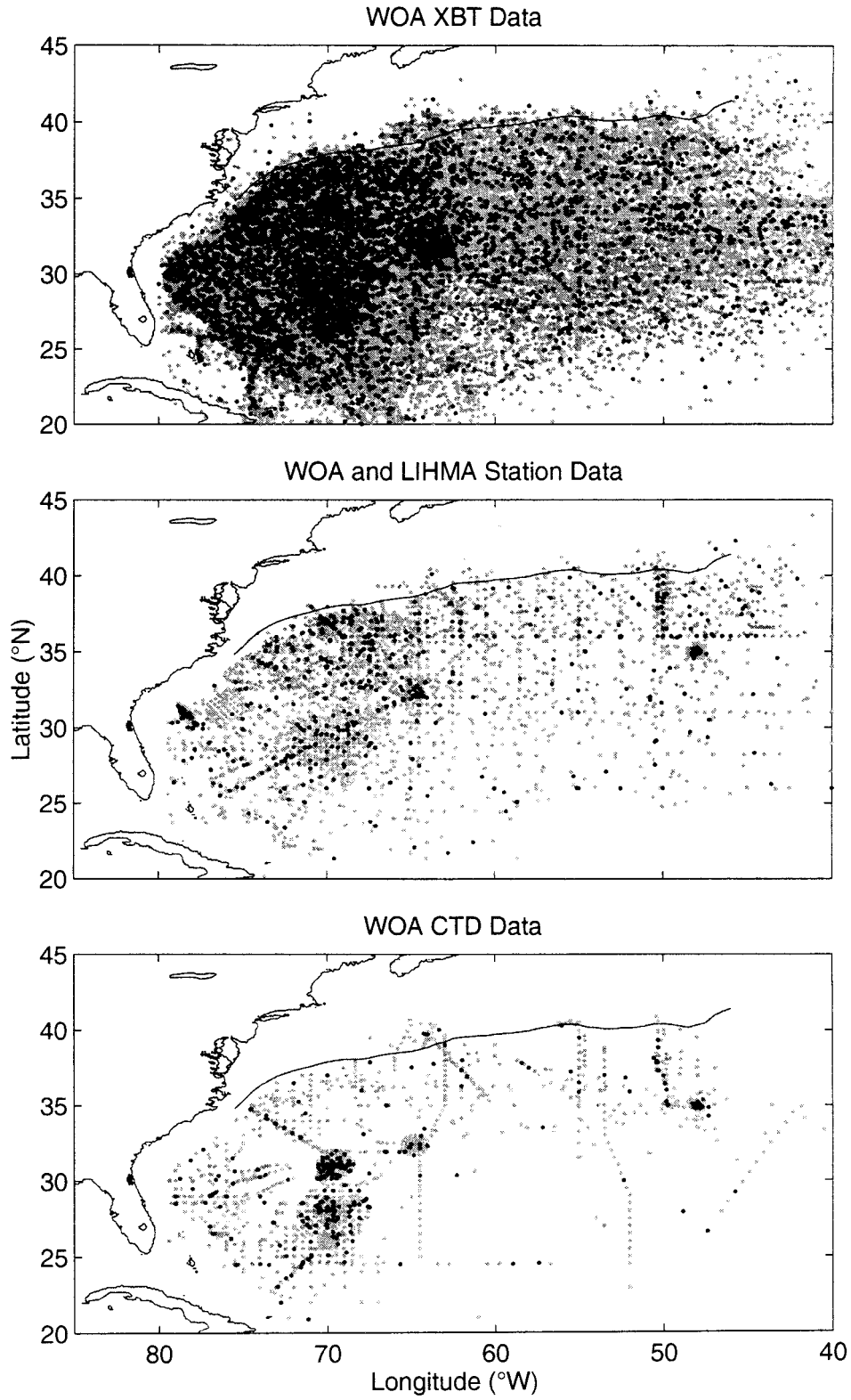WOA and LIHMA Station Data

WOA CTD Data

FIG. 4. Spatial distribution of hydrographic data containing an STMW layer. The solid line extending from Cape Hatteras to the northeast in each plot is the mean position of the north wall of the Gulf Stream, based on 12 yr of satellite sea surface temperature data.
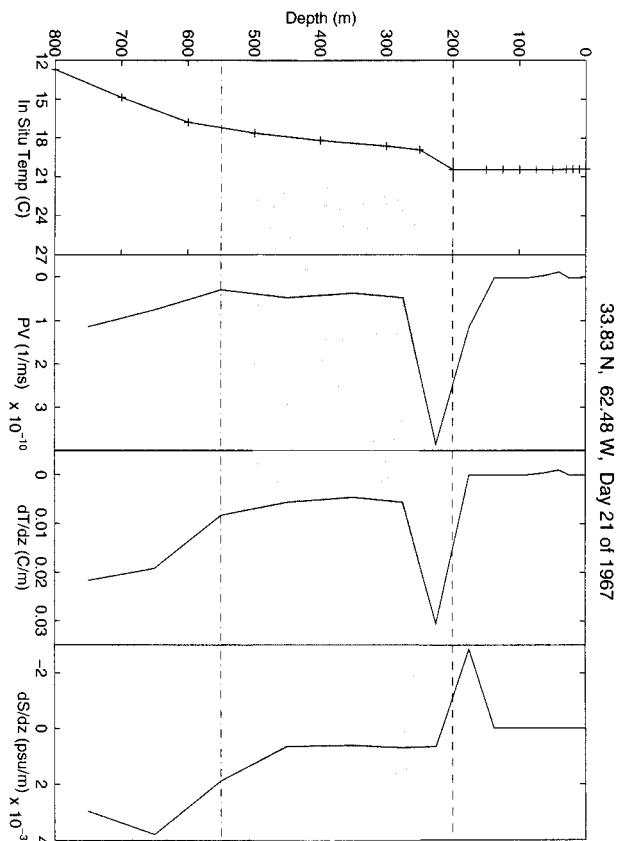
FIG. 5. Example CTD profile showing potential vorticity minimum below the STMW layer identified using temperature alone. The dashed line represents mixed layer depth. The shaded region represents STMW layer. The dashed–dotted line indicates depth of potential vorticity minimum.

TABLE 2. Comparison of properties at the potential vorticity minimum with the STMW layer. The temperature, salinity, and potential density of the STMW layer are weighted means of all values found within the layer. The temperature gradient of the STMW layer was found from the slope of a linear least squares fit to all points in the layer, while the potential vorticity of the STMW layer was found using Eq. (2). See section 4a for details.

	PV minimum within STMW layer		
	PV minimum		STMW layer
Depth (m)	324	Top depth	208
		Bottom depth	416
Temperature (°C)	17.82		17.88
Salinity (psu)	36.46		36.47
σ_θ	26.45		26.44
PV ($\times 10^{-11}$ m^{-1} s^{-1})	4.06		6.05
$\dfrac{\Delta T}{\Delta z}$ [°C (100 m)$^{-1}$]	0.40		0.47

	PV minimum below STMW layer		
	PV minimum		STMW layer
Depth (m)	449	Top depth	222
		Bottom depth	384
Temperature (°C)	16.99		18.03
Salinity (psu)	36.33		36.47
σ_θ	26.55		26.40
PV ($\times 10^{-11}$ m^{-1} s^{-1})	5.70		8.85
$\dfrac{\Delta T}{\Delta z}$ [°C (100 m)$^{-1}$]	0.93		0.58

component of potential vorticity, Eq. (1) (McCartney 1982; Talley and Raymer 1982; Ebbesmeyer and Lindstrom 1986; Klein and Hogg 1996). To verify that the process used here correctly found this stratification minimum, the potential vorticity minima for all station (*WOA94* and Russian) and CTD profiles were compared with the STMW layer found using temperature alone. The potential vorticity minimum was required to be deeper than 100 m to avoid finding the potential vorticity minimum in the surface mixed layer. Over 7500 profiles with maximum depths greater than 600 m found an STMW layer and a potential vorticity minimum. The potential vorticity minimum was within the STMW layer identified using temperature alone in 84% of these profiles. Ten percent of the profiles had the potential vorticity minimum below the STMW layer, while 6% had the potential vorticity minimum above the STMW layer. Nearly all of the profiles with the potential vorticity minimum above the STMW layer occurred in January through April, in a thickening mixed layer (deeper than 100 m) above an older STMW layer from a previous winter, that is, the first STMW configuration. In most of the profiles with the potential vorticity minimum

below the STMW layer, the potential vorticity profile was very uniform with only a slight difference between the potential vorticity minimum and the potential vorticity within the STMW layer. In most of these cases, the potential vorticity minimum was only one depth level below the bottom of the STMW layer selected, based on temperature alone, and was caused by an increasing salinity gradient compensating an increasing temperature gradient. This caused the potential density to be more uniform to deeper depths than either temperature or salinity alone. Figure 5 is an example of such a profile; the method based on temperature alone described above found the layer with the most uniform temperature *and* salinity, the likely remnant of a convectively mixed layer, while the potential vorticity minimum was in a layer of decreasing temperature and salinity.

Table 2 compares the temperature, salinity, and temperature gradient at the potential vorticity minimum with the mean temperature, salinity, and temperature gradient within the STMW layer selected based on temperature alone. When the potential vorticity minimum was within the STMW layer, the two methods agreed very well. When the potential vorticity minimum was below the selected STMW layer, the temperature and salinity of the STMW layer still agreed with typical STMW values [17.9° ± 0.3°C, 36.5 ± 0.1%, ~26.4 km m^{-3} (Worthington 1959)], although the STMW layer was shallower, warmer, less dense, and weaker (more stratified) than when the potential vorticity minimum
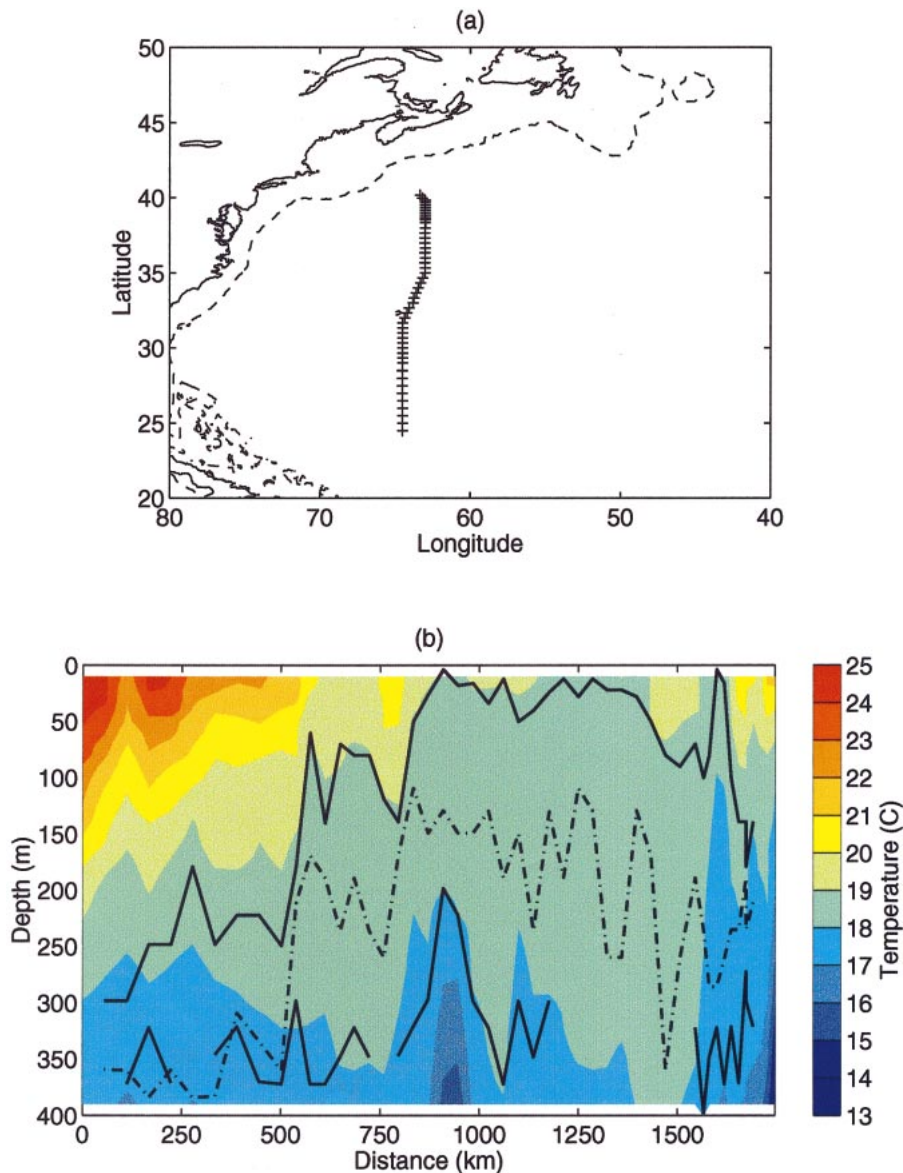
FIG. 6. CTD hydrographic section collected on 17–26 Apr 1985. (a) Locator map: crosses represent stations along section, dotted line represents the 500-m isobath. (b) Temperature distribution along section: solid lines represent the top and bottom of the STMW layer, dashed–dotted line indicates depth of the potential vorticity minimum.

was within the STMW layer. More importantly, the temperature and salinity at the potential vorticity minimum were colder and fresher than typical STMW values, and the mean temperature gradient was almost twice the temperature gradient in the STMW layer above.

Finally, the two methods were applied to a north–south section of CTD data collected along 63°W–64.5°W from 25°N to 40°N on 17–26 April 1985, as shown in the upper panel of Fig. 6. The lower panel shows the temperature distribution along this section along with the depths of the top and bottom of the STMW layer identified by the temperature-based criteria

and the potential vorticity minimum. The maximum depth at each station along the section was 400 m. Therefore, there are some stations along this section where the temperature-based criteria could not find the bottom of the STMW layer before the bottom of the station. Again, the potential vorticity minimum lies within the STMW layer determined using the temperature-based criteria for most of the section, except for the northern part of the section where the STMW layer lies beneath the Gulf Stream and the potential vorticity minimum tends to be deeper than the bottom of the STMW layer found using temperature alone. The po-

tential vorticity minimum, however, is again located in waters less than 17.5°C, while the temperature-based criteria selected a STMW layer with temperatures between 17.5° and 18.5°C.

In summary, using temperature alone, this method identified the deepest, thickest, most uniform layer with STMW characteristics. The potential vorticity (i.e., the stratification) minimum was within this STMW layer in most of the station and CTD profiles. In cases where they did not agree, this method either distinguished the older STMW layer below from the developing STMW layer or it found the likely remnant of the previous winter's convective mixing.

5. Assembling climatologies

The selected hydrographic data are unevenly distributed in space and time. Large amounts of data were collected during times of specific cruises or experiments, with less data collected at other times and places. Therefore, climatologies constructed by finding the straight average of all observations in a given region will be biased toward those years with large data volumes. For example, 1082 of the 3977 (~27%) profiles in the 2.5° lat × 5° long box bounded by 30°N to 32.5°N and 65°W to 70°W were collected in 1978, most in May through August during the POLYMODE Local Dynamics Experiment, an intensive data collection effort aimed at examining the mesoscale variability of the subtropical gyre recirculation (Taft et al. 1986). Therefore, any statistics for this box would be biased toward the summer of 1978. Since these 1000 profiles may not represent 1000 independent samples of the STMW layer, they should not be weighted uniformly when averaged with the remaining profiles from the summer months of other years.

To find an unbiased estimate of the climatological STMW properties in this study, all profiles collected close in time and space were grouped into one cluster, and averaged into one independent observation. The time and length scales used to group the data were chosen based on previously published estimates of the autocorrelation function zero-crossing scales from the POLYMODE Local Dynamics Experiment. Based on the results of Taft et al. (1986), Rossby et al. (1986), Shen et al. (1986), and Ebbesmeyer and Lindstrom (1986), the shortest observed time and spatial autocorrelation zero-crossings (75 km and 10 days) were chosen as the scales to cluster the profiles here. While the decorrelation temporal and spatial scales of the STMW layer will likely vary in time and space and may have longer decorrelation scales, the POLYMODE results were obtained in a relatively high energy region of the subtropical gyre (Rossby et al. 1986; Shen et al. 1986; Taft et al. 1986), and the STMW layer is therefore unlikely to have decorrelation scales much shorter than the ones chosen here.

Following Casey and Cornillon (1999), an agglom-erative hierarchical clustering algorithm (Gong and Richman 1995) was used to find the profiles that were within 75 km and 10 days of each other. This type of clustering process builds up clusters from the set of individual profiles "by the process of accumulation," and yields "hard clusters" wherein each profile is either in or out of a cluster with no overlap between clusters (Gong and Richman 1995). The similarity measurement used here to determine if a profile belonged in a cluster was its "distance" from the profile specified as the cluster center. This distance was determined using the differences in time and space from the center profile:

$$\text{distance} = \sqrt{\Delta x^2 + \Delta y^2 + \Delta t^2}, \quad (3)$$

where Δx and Δy are the x and y distances in kilometers from the center profile, and Δt is the temporal difference between the profile and the center profile, scaled to kilometers, that is,

$$\Delta t = \frac{\text{difference in days} \times \text{spatial clustering radius}}{\text{temporal clustering radius}}.$$
$$(4)$$

This distance (Eq. 3) from a center profile had to be less than 37.5 km in order for a profile to be grouped with the center profile. This requirement meant all profiles within 37.5 km and on the same day of the center profile were grouped together, while profiles 5 days before or after the center profile would have to have Δx and Δy equal zero (i.e., at the same location) in order to be grouped with the center profile.

The seed points needed to initialize the algorithm were chosen sequentially from the dataset (Gong and Richman 1995); each profile was chosen as a cluster center and all profiles meeting the similarity criteria were grouped into a cluster. The initial clusters were then sorted by number of profiles in the cluster and the mean distance of the profiles in the cluster from the center profile. The cluster with the most profiles and smallest mean distance from the center profile was first in this sorted file while individual profiles not belonging to any cluster were last. These sorted clusters were then reevaluated to maximize the number of profiles in a cluster and to ensure no profile was used in more than one cluster.

The mean values for a given area were determined from the weighted mean of all independent observations (clusters and other independent profiles not falling within a cluster) in that area. The estimated error of each cluster mean or individual profile was used as the weighting factor:

$$\overline{X} = \frac{\sum_{i=1}^{N} \dfrac{x_i}{\sigma_i^2}}{\sum_{i=1}^{N} \dfrac{1}{\sigma_i^2}}, \quad (5)$$

where $\overline{X}$ is the mean value for a given area, x_i is ith

independent observation (cluster mean or individual profile), σ_i is the estimated error of the ith independent observation, and N is the number of independent observations in the given area. The uncertainty of the mean ($\sigma_{\bar{X}}^2$) is then given by

$$\frac{1}{\sigma_{\bar{X}}^2} = \sum_{i=1}^{N} \frac{1}{\sigma_i^2}. \tag{6}$$

In order to estimate the error for the cluster means, the variance within a group of XBT, station, and CTD profiles was split into three components:

1) the uncertainty due to random errors in the dataset, σ_{error}, which lead to an incorrect determination of the STMW layer (e.g., right panel of Fig. 3) such as:
   (a) instrument uncertainties that are introduced as the data are acquired by each measurement technique (e.g., reading deep sea reversing thermometers and analog XBT traces);
   (b) subsampling the temperature profile using inflection points, a fixed depth interval, or standard depths; and
   (c) errors introduced between the original data acquisition and archival at the NODC OCL;
   because these errors are assumed to be random, the magnitude of the uncertainty decreases as the number of observations averaged together increases;
2) the geophysical variability within a cluster of correlated profiles [i.e., scales less than the approximate decorrelation timescales and space scales (10 days, 75 km)]. This will be called the small scale geophysical variability, σ_{small}.
3) the geophysical variability between decorrelated and therefore independent samples (i.e., scales larger than the approximate decorrelation scales). This will be called the large scale geophysical variability, σ_{large}.

Using this notation and Eq. (6), the variance of the weighted mean for the parameter of interest for the jth cluster is

$$\frac{1}{\sigma_M^2} = \sum_{i=1}^{M} \frac{1}{\sigma_{\text{small}}^2 + \sigma_{\text{error}_i}^2}, \tag{7}$$

and the uncertainty of the weighted mean of N clusters is:

$$\frac{1}{\sigma_N^2} = \sum_{j=1}^{N} \frac{1}{\sigma_{\text{clust}_j}^2} = \sum_{j=1}^{N} \frac{1}{\sigma_{\text{large}}^2 + \sigma_{M_j}^2}. \tag{8}$$

If the small scale geophysical variability is much larger than the random error uncertainty in the XBT, CTD, and station profiles, then each independent observation should have an equal weighting. However, if the random error uncertainty in the XBT, CTD, and station profiles is greater than the small scale geophysical variability and differs from one instrument to another, then each independent observation should have a different weight which is dependent on its random error uncertainty. Therefore, in order to weight each cluster of mixed in-

strument types appropriately, each of these variances must be estimated.

The random error uncertainty was determined by clustering XBT, station, and CTD profiles separately using the 75-km and 10-day criteria. For XBT and station clusters, the random error uncertainty was chosen as the median of the cluster standard deviations for clusters with a mean distance from the center profile less than 10 km. While the cluster standard deviations tended to be scattered, the standard deviations of XBT and station clusters with mean distances from center less than 10 km were typically smaller than the standard deviations of clusters with larger mean distances from center. The variability between profiles at these small time and space scales will be due more to random error uncertainty than geophysical variability. Because the CTD data were the most heavily clustered dataset, there were not sufficient clusters with mean distances from the center profile less than 10 km to determine a representative random error uncertainty. Since the CTD cluster standard deviations tended to vary less with the cluster mean distance from the center profile than the XBT or bottle clusters, the CTD random error uncertainty was chosen as the median of all CTD cluster standard deviations. Only clusters containing four or more profiles were included in these distributions.

The small and large scale geophysical variabilities were determined by first finding clusters of all profiles (XBT, CTD, and station) that were within 75 km and 10 days of each other. Each profile in a cluster was demeaned by subtracting the cluster mean from the profile's value. The small scale geophysical variability was estimated by subtracting the mean random error variance from the variance of the distribution of demeaned profiles:

$$\sigma_{\text{small}}^2 = \sigma_{\text{demeaned}}^2 - \frac{1}{N} \sum_{j=1}^{N} \sigma_{\text{error}_j}^2. \tag{9}$$

Again, only clusters containing four or more profiles were included in this distribution. The large scale geophysical variability was estimated by subtracting the mean variance between profiles within the clusters (i.e., the sum of the random error and small scale geophysical variances) from the total variance of the cluster averages:

$$\sigma_{\text{large}}^2 = \sigma_N^2 - \frac{1}{N} \sum_{i=1}^{N} \frac{\sigma_{M_i}^2}{M_i}. \tag{10}$$

Following the clustering procedure outlined here, the 74 127 CTD, XBT, and station profiles listed in Table 1 yielded a total of 42 771 independent observations. Using the region from 30°N to 32.5°N and 65°W to 70°W again as an example, the 3977 profiles collected in this region yielded a total of 1887 independent observations, while the 1082 profiles collected in this region in 1978 yielded 286 independent observations. The clustering done here, then, reduced the weight given to

the profiles collected in this region in 1978 by about half, from ~27% to ~15%.

6. Average STMW layer characteristics

Several authors have demonstrated that dynamical processes associated with small temporal and spatial scale features such as eddies and cold core rings have an impact on the STMW layer (e.g., Brundage and Dugan 1986; Ebbesmeyer and Lindstrom 1986). Although these small scale dynamical features must play some role in determining the long-term distribution of properties in the STMW layer, the distribution of the data in the *WOA94* prevents us from assessing their impact and relative importance here. The goal here, instead, is to examine the average spatial distribution of STMW layer properties found in the previously described climatology. The 1968–1988 average top and bottom depth and temperature, temperature gradient, and average temperature of the STMW layer are determined every 2.5° and 5.0°. These years were chosen based on data availability. The beginning of this interval was defined by the rapid increase in the use of XBT probes for data collection, while its end was defined by the fall off of XBT data available from NODC, due to the time lag between data collection and submission to NODC for archival.

To eliminate the effect of seasonal changes in the properties at the top of the STMW layer (shoaling in February–April, deepening after May) on the long-term averages, clusters–profiles from September through December are used here to determine the mean STMW properties. The seasonal pycnocline is at its deepest during these months, therefore there is minimal reentrainment of the waters at the top of the STMW layer back into the mixed layer. The averages presented here, then, represent the mean STMW layer which is the remnant of the previous winter's convective mixing, and is the STMW layer available for possible renewal in the next winter.

The mean and standard deviation of each of the STMW layer properties were first determined from the September–December clusters–profiles for each year in 2.5° lat × 5° long bins using Eqs. (5) and (6). The annual means for each bin were then averaged. In this averaging, each year's annual mean was again weighted by its standard error, and the mean and standard error for each bin were found using Eqs. (5) and (6). Averages were not found for bins with fewer than five annual means. Finding the STMW mean properties in this way has two advantages. First, it minimizes biasing the means toward years with large data volumes. Second, the interannual variability in the STMW properties can be estimated from the variance of the annual means about their average.

Yasuda and Hanawa (1997) used a similar approach in constructing their two decadal climatologies of North Pacific STMW. They found annual seasonal averages in 2° × 2° bins, then averaged the annual means. The slightly coarser bin size used here is needed to ensure reliable estimates of the mean depth and temperature of the bottom of the STMW layer as well as the average temperature of the layer since these properties were only determined from those profiles with maximum depths greater than 600 m. This requirement reduced the number of data points available to determine the means for these properties by ~⅔.

a. Depth

The mean depth of the top and bottom of the STMW layer are shown in Fig. 7. Bins with either no data or data in fewer than 5 yr are shaded gray. The standard errors for the STMW top and bottom depths are less than 10 m, and are uniformly distributed over almost the entire region. From Fig. 7, the STMW layer is deeper and thicker to the west than to the east. Thickness ranges from ~175 m in the east to ~200 m in the west. Since the bottom depth contours are oriented primarily north–south while the top depth contours south of 30°N are oriented primarily east–west, deepening to the south, the STMW layer becomes thinner to the south of 30°N.

These results are in general agreement with previous observations of STMW in individual hydrographic sections, which found the STMW arriving at Bermuda was between the depths of 150 and 450 m (Schroeder et al. 1959); and the STMW layer was nominally 200 m thick with greatest thickness (>250 m) just south of the Gulf Stream (Schroeder et al. 1959; Worthington 1959; Istoshin 1961; Leetmaa 1977; Worthington 1977; Talley and Raymer 1982; Ebbesmeyer and Lindstrom 1986; Taft et al. 1986); thickness decreasing to the south, particularly south of 32°N (Istoshin 1961; Suga et al. 1989); and decreasing from west to east (Masuzawa 1972; Hanawa 1987).

b. Temperature

The mean temperatures at the top and bottom of the STMW layer are shown in Fig. 7, while the average temperature of the layer is shown in Fig. 8. The standard errors for the STMW top temperature are less than 0.05°C, and are again uniformly distributed over almost the entire region, while they range from 0.05° to 0.1°C for the bottom temperature, with the smaller errors west of 60°W than east. The standard errors for the average temperature range from 0.05° to 0.1°C, with smaller errors again west of 60°W than east.

There is good agreement between the average temperature of the STMW layer in Fig. 8 and Worthington's (1959) original "classical" definition of the STMW temperature, 17.9° ± 0.3°C. The vertical temperature difference through the layer ranges from 0.8° to 1.0°C (Fig. 7).

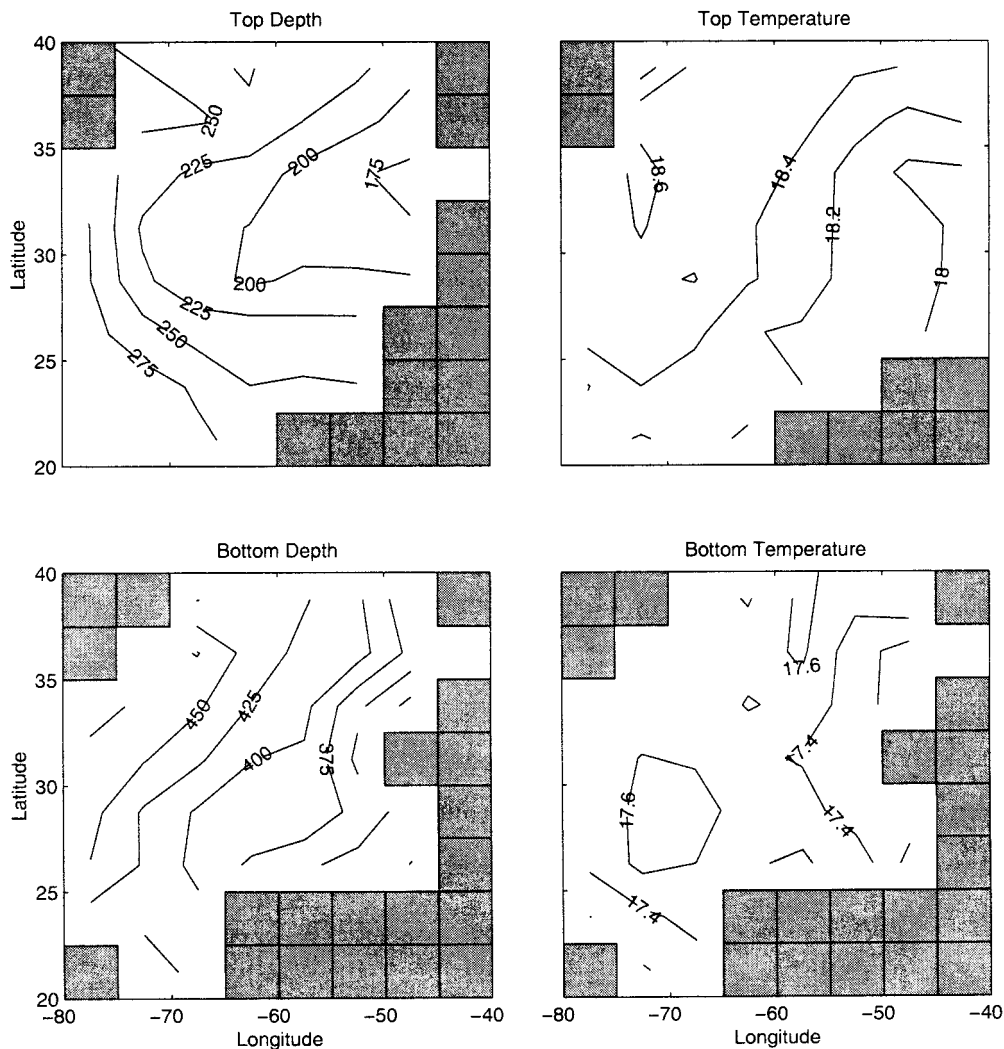The east–west gradient in the temperature of the STMW layer (colder to the east, warmer to the west)

FIG. 7. Contoured 2.5° lat × 5.0° long mean STMW top and bottom depths (m) and temperatures (°C). The contour intervals are more than twice as large as the standard errors for the depths (<10 m) and temperatures (<0.1°C) over most of the region.

is readily evident in both figures. This gradient is larger at the top of the STMW layer (~0.4°–0.6°C across the gyre) than at the bottom (~0.2°–0.4°C across the gyre). This east–west temperature gradient has been widely reported by others (McCartney et al. 1980; Talley and Raymer 1982; Ebbesmeyer and Lindstrom 1986; Hall and Fofonoff 1993; Klein and Hogg 1996), but only in individual or pairs of hydrographic sections. The previously reported east–west temperature differences range from 0.6°C from 68°W to 53°W (Talley and Raymer 1982) to 0.9°C from 68°W to 55°W (Hall and Fofonoff 1993). These east–west gradients have been observed in newly formed NASTMW (Talley and Raymer 1982; Hall and Fofonoff 1993), and persist as the STMW is advected through the subtropical gyre (Ebbesmeyer and Lindstrom 1986; Klein and Hogg 1996). Because these east–west temperature gradients are persistent features of the STMW layer, the temperature dif-

ferences seen in this climatology (Fig. 7) are comparable to these instantaneous values.

c. Temperature gradient

The mean temperature gradient through the STMW layer is shown in Fig. 8. The standard errors for the temperature gradient range from 0.01° to 0.025°C (100 m)$^{-1}$, with the smaller errors again west of 60°W than east. On average, the STMW layer in September through December has a temperature gradient of 0.5°–0.55°C (100 m)$^{-1}$ with the gradient through the layer increasing to the south of 30°N. Therefore, a 150–200-m-thick STMW layer (Fig. 7) will again have a temperature difference through it of ~0.8°–1.1°C.

Other observations of the temperature gradient through the STMW layer range from 0.3°C (100 m)$^{-1}$ in recently renewed STMW (McCartney et al. 1980) to
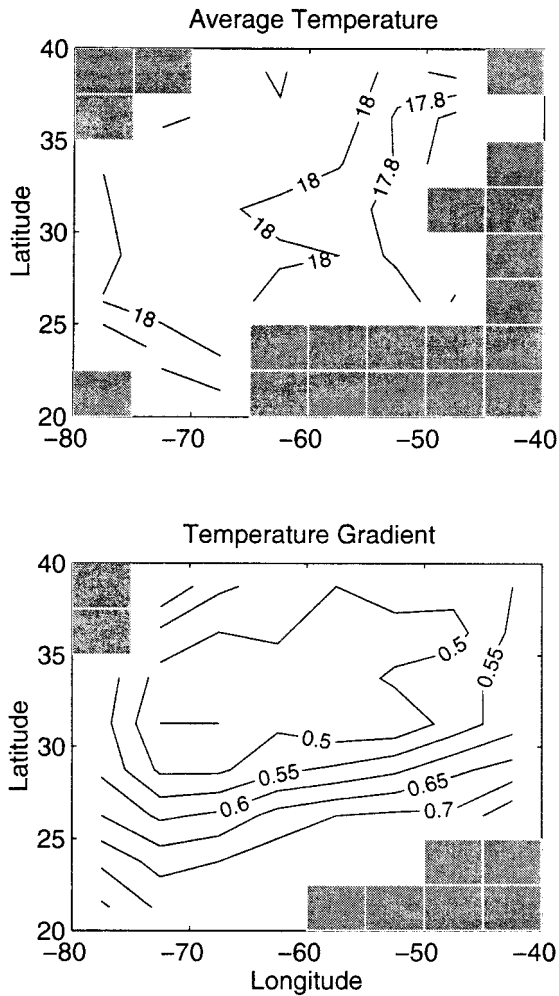
Average Temperature

Temperature Gradient

FIG. 8. Contoured 2.5° lat × 5.0° long mean STMW average temperature (°C) and temperature gradient [°C (100 m)$^{-1}$]. The contour intervals are more than twice as large as the standard errors for the average temperature (<0.1°C) and temperature gradient [<0.025°C (100 m)$^{-1}$] over most of the region.
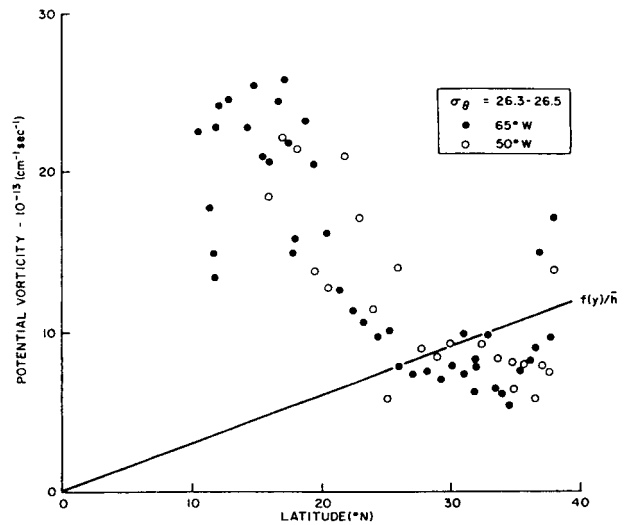

FIG. 9. Potential vorticity computed between the $\sigma_\theta = 26.3$ and 26.5 surfaces at individual stations along 65°W and 50°W, from Mc-Dowell et al. (1982).

and 27.3–27.6 isopycnal surfaces in the North Atlantic. The density of the minimum potential vorticities found here (Table 2) falls within the 26.3 to 26.5 layer. Their Fig. 17 showing potential vorticity in this layer as a function of latitude is reproduced here in Fig. 9. First, the mean minimum potential vorticity of the STMW layers found in this study with potential densities between 26.3 and 26.5, and from 25°N to 35°N (3020 profiles), was 6.13×10^{-11} m^{-1} s^{-1}, which corresponds well with the values in the region of relatively constant potential vorticities between these latitudes in Fig. 9. Second, the variation of potential vorticity with latitude in Fig. 9 mimics the change in the temperature gradient through the STMW layer with latitude shown in Fig. 8. Both show a plateau of homogeneous values to the north of ~ 29°N and a rapid increase to the south of ~ 29°N.

The features shown in Fig. 8 (region of uniform temperature gradients south of the western boundary current with a "ramp" of rapidly increasing temperature gradients farther to the south) also agree with the results of Rhines and Young's (1982) theory of potential vorticity homogenization in unventilated layers of planetary gyres. Their theory predicts a pool of homogenized potential vorticity created by weak horizontal diffusion down the potential vorticity gradient, if the wind-driven motion above the unventilated layer is strong enough to cause lines of constant potential vorticity to close on themselves. Outside this homogenized region, the potential vorticity contours tend to be oriented east–west. In support of their hypothesis, they presented the unpublished results of a 3-layer numerical model of the wind-driven circulation by W. B. Holland. The potential vorticity structure of the middle, unventilated region [Rhines and Young (1982), Fig. 3] again compares well with Fig. 8, showing a plateau of homogeneous potential vorticity south of the western boundary current and a

0.8°C (100 m)$^{-1}$ in STMW with no recent exposure to convective mixing (Worthington 1977). Klein and Hogg (1996) found by comparing *Panulirus* hydrographic data collected in the vicinity of Bermuda with XBT data, that the STMW layer near Bermuda was associated with temperature gradients less than 0.8°C (100 m)$^{-1}$. Again, the mean values shown in Fig. 8 are comparable to these instantaneous observations of the STMW layer temperature gradient.

There are no previous observations of the spatial variations in the temperature gradient through the STMW layer. McCartney (1982), however, did note that the potential vorticity (potential density gradient) of the STMW layer does increase to the south, which agrees with the increase in the temperature gradient to the south seen here. In addition McDowell et al. (1982) mapped the variation of potential vorticity calculated between the $\sigma_\theta = 26.0$–26.3, 26.3–26.5, 26.5–27.0, 27.0–27.3,

ramp of rapidly changing potential vorticity oriented east–west south of the pool of homogenized potential vorticity.

Rhines and Young's (1982) model was of an unventilated layer isolated from direct atmospheric forcing. The STMW layer can be exposed to direct atmospheric cooling during renewal years, and is thus not strictly unventilated. Dewar (1986) examined the potential vorticity structure of a "weakly" ventilated layer by allowing a small region within the closed potential vorticity contours to experience diabatic forcing driven by surface heat exchange. His results found a homogenized potential vorticity region at the center of the closed geostrophic contours (which was a local minimum and corresponded to the unventilated region within the closed geostrophic contours) and a "bowl-shaped region" near the edges of the region of closed geostrophic contours where the potential vorticity increased due to the diabatic forcing.

There is some indication in Fig. 8 that the temperature gradients do increase on the northern, eastern, and western edges of the plateau of homogeneous temperature gradients. At this point, however, the ramp of increasing temperature gradients to the south seems to be a more prevalent feature. The difference between the STMW layer here and Dewar's weakly ventilated layer is that, in Dewar's model, the diabatic forcing was always acting on the layer, whereas in the STMW layer the diabatic forcing acts on the layer for a limited amount of time. Comparing Fig. 8 to Dewar's results, then, seems to suggest that the STMW layer behaves more as an unventilated layer than a ventilated layer once it has been isolated from the atmosphere by the seasonal thermocline.

7. Conclusions

The method used here for identifying the STMW layer using temperature profiles alone is comparable to identifying the STMW layer as the stratification minimum. This temperature-based method, however, has the added advantage of being able to use XBTs which have a much denser spatial and temporal distribution than CTDs and station data. On average, the STMW layer, which is the remnant of the previous winter's convective mixing, is found between 175 and 450 m, has an average temperature near 18°C, and a temperature gradient of $0.5°C (100 \text{ m})^{-1}$. The spatial distribution of these properties agrees with previous observations of the STMW layer. The north–south variations in the STMW layer temperature gradient correspond with observations of potential vorticity, as well as numerical model results of the potential vorticity structure of an unventilated layer with weak horizontal diffusion. The companion to this paper (Alfultis and Cornillon 2001) will use the results from this temperature-based method of determining STMW properties to examine the annual and interannual variability in the STMW layer characteristics and structure.

REFERENCES

Alfultis, M., 1997: Statistical characterizations of North Atlantic Subtropical Mode Water. Ph.D. dissertation, University of Rhode Island, 161 pp.

——, and P. Cornillon, 2001: Annual and interannual changes in the North Atlantic STMW layer properties. *J. Phys. Oceanogr.,* **31,** 2066–2086.

Belkin, I., and A. Gordon, 1996: Southern Ocean fronts from the Greenwich meridian to Tasmania. *J. Geophys. Res.,* **101** (C2), 3675–3696.

Bingham, F. M., 1992: Formation and spreading of subtropical mode water in the North Pacific. *J. Geophys. Res.,* **97,** 11 177–11 189.

Brundage, W. L., and J. P. Dugan, 1986: Observations of an anticyclonic eddy of 18° water in the Sargasso Sea. *J. Phys. Oceanogr.,* **16,** 717–727.

Casey, K. S., and P. Cornillon, 1999: A comparison of satellite and in situ–based sea surface temperature climatologies. *J. Climate,* **12,** 1848–1863.

Dewar, W. K., 1986: On the potential vorticity structure of weakly ventilated isopycnals: A theory of subtropical mode water maintenance. *J. Phys. Oceanogr.,* **16,** 1204–1216.

Ebbesmeyer, C., and E. Lindstrom, 1986: Structure and origin of 18°C water observed during the POLYMODE local dynamics experiment. *J. Phys. Oceanogr.,* **16,** 443–453.

Gong, X., and M. B. Richman, 1995: On the application of cluster analysis to growing season precipitation data in North America east of the Rockies. *J. Climate,* **8,** 897–931.

Hall, M., and M. Fofonoff, 1993: Downstream development of the Gulf Stream from 68° to 55°W. *J. Phys. Oceanogr.,* **23,** 225–249.

Hallock, Z., and W. Teague, 1992: The fall rate of the T-7 XBT. *J. Atmos. Oceanic Technol.,* **9,** 470–483.

Hanawa, K., 1987: Interannual variations of the winter-time outcrop area of Subtropical Mode Water in the western North Pacific Ocean. *Atmos.–Ocean,* **25,** 358–374.

——, and H. Yoritaka, 1987: Detection of systematic errors in XBT data and their correction. *J. Oceanogr. Soc. Japan,* **43,** 68–76.

——, and I. Hoshino, 1988: Temperature structure and mixed layer in the Kuroshio region over the Izu Ridge. *J. Mar. Res.,* **46,** 683–700.

——, and Y. Yoshikawa, 1991: Reexamination of the depth error in XBT data. *J. Atmos. Oceanic Technol.,* **8,** 422–429.

——, P. Rual, R. Bailey, A. Sy, and M. Szabados, 1995: A new depth-time equation for Sippican or TSK T-7, T-6, and T-4 expendable bathythermographs (XBT). *Deep-Sea Res.,* **42,** 1423–1451.

Hazeleger, W., and S. Drijfhout, 1998: Mode water variability in a model of the subtropical gyre: Response to anomalous forcing. *J. Phys. Oceanogr.,* **28,** 266–288.

Istoshin, Y., 1961: Formative area of 'eighteen-degree' water in the Sargasso Sea. *Deep-Sea Res.,* **9,** 384–390.

Joyce, T. M., and P. Robbins, 1996: The long-term hydrographic record at Bermuda. *J. Climate,* **9,** 3121–3131.

Klein, B., and N. Hogg, 1996: On the interannual variability of 18 Degree Water formation as observed from moored instruments at 55°W. *Deep-Sea Res.,* **43,** 1777–1806.

Lamb, P., 1984: On the mixed-layer climatology of the North and Tropical Atlantic. *Tellus,* **36A,** 292–305.

Lappo, S., G. Alekseev, and V. Efimov, 1995: On oceanological results of the program Sections. *Atmos. Oceanic Phys.,* **31,** 373–384.

Leetmaa, A., 1977: Effects of the winter of 1976–1977 on the northwestern Sargasso Sea. *Science,* **198,** 188–189.

Levitus, S., and T. P. Boyer, 1994: *Temperature.* Vol. 4, *World Ocean Atlas 1994,* NOAA Atlas NESDIS, 117 pp.

Marsh, R., and A. L. New, 1996: Modeling 18° Water variability. *J. Phys. Oceanogr.,* **26,** 1059–1080.

Masuzawa, J., 1969: Subtropical mode water. *Deep-Sea Res.,* **16,** 463–472.

——, J., 1972: Water characteristics of the North Pacific central region. *Kuroshio: Its Physical Aspects,* H. Stommel and K. Yoshida, Eds., University of Tokyo Press, 95–127.

McCartney, M., 1982: The subtropical recirculation of mode waters. *J. Mar. Res.,* **40** (Suppl.), 427–464.

——, L. Worthington, and M. Raymer, 1980: Anomalous water mass distributions at 55°W in the North Atlantic in 1977. *J. Mar. Res.,* **38,** 147–172.

McDowell, S., P. Rhines, and T. Keffer, 1982: North Atlantic potential vorticity and its relation to the general circulation. *J. Phys. Oceanogr.,* **12,** 1417–1436.

Provost, C., C. Escoffier, K. Maamaatuaiahutapu, A. Kartavtseff, and V. Garcon, 1999: Subtropical Mode Waters in the South Atlantic Ocean. *J. Geophys. Res.,* **104,** 21 033–21 049.

Qiu, B., and T. Joyce, 1992: Interannual variability in the mid- and low-latitude western North Pacific. *J. Phys. Oceanogr.,* **22,** 1062–1079.

Rhines, P. B., and W. R. Young, 1982: Homogenization of potential vorticity in planetary gyres. *J. Fluid Mech.,* **122,** 347–367.

Roemmich, D., and B. Cornuelle, 1992: The Subtropical Mode Waters of the South Pacific Ocean. *J. Phys. Oceanogr.,* **22,** 1178–1187.

Rossby, T., J. Price, and D. Webb, 1986: The spatial and temporal evolution of a cluster of SOFAR floats in the POLYMODE Local Dynamics Experiment (LDE). *J. Phys. Oceanogr.,* **16,** 428–442.

Schroeder, E., H. Stommel, D. Menzel, and W. Sutcliffe Jr., 1959: Climatic stability of eighteen degree water at Bermuda. *J. Geophys. Res.,* **64,** 363–366.

Shen, C. Y., J. C. McWilliams, B. A. Taft, C. C. Ebbesmeyer, and E. J. Lindstrom, 1986: The mesoscale spatial structure and evolution of dynamical and scalar properties observed in the northwestern Atlantic Ocean during the POLYMODE Local Dynamics Experiment. *J. Phys. Oceanogr.,* **16,** 454–482.

Singer, J., 1990: On the error observed in electronically digitized T-7 XBT data. *J. Atmos. Oceanic Technol.,* **7,** 603–611.

Suga, T., and K. Hanawa, 1990: The mixed layer climatology in the northwestern part of the North Pacific subtropical gyre and the formation area of Subtropical Mode Water. *J. Mar. Res.,* **48,** 543–566.

——, and ——, 1995: Interannual variations of North Pacific Subtropical Mode Water in the 137°E section. *J. Phys. Oceanogr.,* **25,** 1012–1017.

——, ——, and Y. Toba, 1989: Subtropical mode water in the 137°E section. *J. Phys. Oceanogr.,* **19,** 1605–1618.

Taft, B. A., E. J. Lindstrom, C. C. Ebbesmeyer, C. Y. Shen, and J. C. McWilliams, 1986: Water mass structure during the POLYMODE Local Dynamics Experiment. *J. Phys. Oceanogr.,* **16,** 403–426.

Talley, L., and M. Raymer, 1982: Eighteen degree water variability. *J. Mar. Res.,* **40** (Suppl.), 757–775.

Worthington, L., 1959: The 18° water in the Sargasso Sea. *Deep-Sea Res.,* **5,** 297–305.

——, 1972: Negative oceanic heat flux as a cause of water-mass formation. *J. Phys. Oceanogr.,* **2,** 205–211.

——, 1977: Intensification of the Gulf Stream after the winter of 1976–77. *Nature,* **270,** 415–417.

Yasuda, T., and K. Hanawa, 1997: Decadal changes in the mode waters in the midlatitude North Pacific. *J. Phys. Oceanogr.,* **27,** 858–870.